Soil denudation rates in an old-growth mountain temperate forest driven by tree uprooting dynamics, Central Europe

Šamonil, Pavel ; Egli, Markus ; Steinert, Teresa ; Norton, Kevin ; Abiven, Samuel ; Daněk, Pavel ; Hort, Libor ; Brandová, Dagmar ; Christl, Marcus ; Tikhomirov, Dmitry

Abstract: Tree uprooting may distinctly affect landscape dynamics and slope denudation. Little is known, however, about the corresponding soil redistribution rates (erosion and accumulation) on either a long-term (millennia; 10Be) or a short-term (decades; 239+240Pu) scale. We determined these rates in a well-investigated forest reserve (Zofinsky primeval forest, Czech Republic) using complementary techniques: nuclides in soils and tors to derive short- to long-term rates and monitoring data (43 years) of repeated tree censuses using tree uprooting data. Temporal trends of soil erosion rates were obtained by dating the timing of exhumation (10Be) of tors. The average long-term denudation rates were about 30–40 t km−2 yr−1. It seems that these rates varied over time with probably a maximum during the Pleistocene/Holocene transition (58–91 t km−2 yr−1). 239+240Pu activities in the soils identified soil redistribution rates of 50 to >100 t km−2 yr−1 for the last decades and agree with results from the tree uprooting monitoring (<92 t km−2 yr−1). In-situ 10Be in soils gave similar denudation rates (58–76 t km−2 yr−1). Meteoric 10Be provided a mean residence time of a soil particle of 33–100 ka supporting the measured average long-term erosion rates. Soil aggregates indicated stable physical conditions meaning that soil mass redistribution occurs only sporadically. It seems that the main driving factors of denudation changed over time. An erosion peak at the Pleistocene/Holocene transition (climate change) seems likely but needs further proof. Over the last few millennia, tree uprooting seems the main driver of soil erosion.

DOI: https://doi.org/10.1002/ldr.3443

LDD Land Degradation & Development

Soil denudation rates in an old-growth mountain temperate forest driven by tree uprooting dynamics, Central Europe

Journal:	*Land Degradation & Development*
Manuscript ID	LDD-19-0351.R2
Wiley - Manuscript type:	Research Article
Date Submitted by the Author:	n/a
Complete List of Authors:	Samonil, P.; The Silva Tarouca Research Institute, Department of Forest Ecology Egli, Markus; University of Zurich, Department of Geography Steinert, Teresa; University of Zurich, Department of Geography Norton, Kevin; Victoria University of Wellington, School of Geography, Environment and Earth Sciences Abiven, S; University of Zurich Faculty of Mathematics and Science, Department of Geography Daněk, Pavel ; The Silva Tarouca Research Institute, Department of Forest Ecology Hort, Libor ; The Silva Tarouca Research Institute, Department of Forest Ecology Brandova, Dagmar; University of Zurich, Department of Geography; Christl, Marcus; ETH Zürich, Department of Physics Tikhomirov, Dmitry ; University of Zurich, Department of Geography
Keywords:	soil erosion, hillslope processes, tree throw pit-mound, beech, spruce

Soil denudation rates in an old-growth mountain temperate forest driven by tree uprooting dynamics, Central Europe

short running title: Soil denudation driven by tree uprooting

Pavel Šamonil[b], Markus Egli[a,*], Teresa Steinert[a], Kevin Norton[c], Samuel Abiven[a], Pavel Daněk[bd], Libor Hort[b], Dagmar Brandová[a], Marcus Christl[e], Dmitry Tikhomirov[ae]

[a] Department of Geography, University of Zurich, Winterthurerstrasse 190, 8057 Zurich, Switzerland

[b] Department of Forest Ecology, The Silva Tarouca Research Institute, Lidická 25/27, Brno 602 00, Czech Republic

[c] School of Earth and Environment, Victoria University of Wellington, PO Box 600, 6140 Wellington, New Zealand

[d] Department of Botany and Zoology, Faculty of Science, Masaryk University, Kotlářská 267/2, 611 37 Brno, Czech Republic

[e] Laboratory of Ion Beam Physics, ETH Zürich, 8093 Zurich, Switzerland

*Corresponding author. Tel.: +41 44 635 51 14; Fax: +41 44 6356848.

E-mail address: markus.egli@geo.uzh.ch (M. Egli).

Pavel Šamonil and Markus Egli share first authorship

Abstract

Tree uprooting may distinctly affect landscape dynamics and slope denudation. Little is known, however, about the corresponding soil redistribution rates (erosion, accumulation), on either a long-term (millennia; ^{10}Be) or a short-term (decades; $^{239+240}$Pu) scale. We determined these rates in a well-investigated forest reserve (Zofinsky primeval forest, Czech Republic) using complementary techniques: nuclides in soils and tors to derive short- to long-term rates and monitoring data (43 years) of repeated tree censuses using tree uprooting data. Temporal trends of soil erosion rates were obtained by dating the timing of exhumation (^{10}Be) of tors. The average long-term denudation rates were about 30–40 t km^{-2} yr^{-1}. It seems that these rates varied over time with probably a maximum during the Pleistocene/Holocene transition (58–91 t km^{-2} yr^{-1}). $^{239+240}$Pu activities in the soils identified soil redistribution rates of 50 to >100 t km^{-2} yr^{-1} for the last decades and agree with results from the tree uprooting monitoring (<92 t km^{-2} yr^{-1}). In-situ ^{10}Be in soils gave similar denudation rates (58–76 t km^{-2} yr^{-1}). Meteoric ^{10}Be provided a mean residence time of a soil particle of 33–100 ka supporting the measured average long-term erosion rates. Soil aggregates indicated stable physical conditions meaning that soil mass redistribution occurs only sporadically. It seems that the main driving factors of denudation changed over time. An erosion peak at the Pleistocene/Holocene transition (climate change) seems likely but needs further proof. Over the last few millennia tree uprooting seems the main driver of soil erosion.

Keywords: soil erosion; hillslope processes; tree throw pit-mound; beech; spruce; biogeomorphology

1 Introduction

Soil losses are due to soil creep, shallow landsliding, debris flow, rotation slumping, water and wind erosion, mineral expansion and contraction and induced movements or thermal processes such as ice-thaw mechanisms giving rise to soli- and gelifluction (e.g., Johnson et al., 2005; Pawlik et al., 2016). Depending on the steepness of the slope, lateral movement of soil material is an important process shaping the landscape (Gabet and Mudd, 2010). Soil creep is considered as a slow displacement that causes soil transport and deformation (Kirkby 1967, 2004). An often-underestimated process in this respect is soil translocation by biotic processes (Phillips, 2009; Strzyzowski et al., 2018; Román-Sánchez et al., 2019) and particularly by trees (Pawlik et al., 2016). Geomorphic reworking and transport of material along slopes, that can even be upslope (cf. tree throw), is often referred to biogenic creep (Lehre, 1987; Pawlik and Šamonil, 2018).

Tree uprooting represents a crucial biomechanical effect of biota in many forested landscapes (Šamonil et al., 2017, 2018). Even in flat areas with no overall lateral movement, uprooting affects main soil characteristics by mixing soil horizons that were originally systematically stratified and redirecting pedogenetical pathways (Schaetzl and Follmer, 1990; Šamonil et al., 2015). In a co-evolutional model, soil formation is characterised by 'progressive' or 'regressive' process groups (Johnson and Watson-Steger 1987). Tree uprooting disrupts the progressive process by soil redistribution (erosion/accumulation) and by affecting the sequence of soil horizons, organic matter decomposition, mineral alteration, leaching, water flow and physical processes.

Forest ecosystems represent the environment having the highest intensity of biogenic creep. For example, Šamonil et al. (2018) estimated that 322 m^3 ha^{-1} of soil is moved by the biomechanical effects of trees in Central European old-growth mountain forests. Although a single tree throw event influences only few square metres with a sharp transition to the surrounded undisturbed soil, they distinctly impact on landscape scale in the long-term. Bormann et al. (1995) determined the so far shortest known 'turnover time' with only 200–400 years in Alaska (USA). This means that the whole soil column is fully bioturbated by tree uprooting every 200–400 years. Central European old-growth mountain forests seem completely uprooted, and thus bioturbated, at average every about 1000–1400 years (Šamonil et al., 2013). In the context of biogenic creep, the biomantle concept was created (Johnson, 2002) that distinguishes three general stages: i) material is

removed from the surface; ii) it may be redeposited along the slope in small pits (caused by bioturbation); and iii) the bioturbation-affected layer slowly migrates downslope with its rate depending on slope angle, intensity and duration of disturbance.

Despite this more general knowledge, the rates of biomechanical processes, their spatial variability and involved time scales are poorly known. In erosion studies and modelling, one usually surmises that erosion is almost zero in forested landscapes (e.g., Meusburger and Alewell, 2014). In the context of high tree-uprooting dynamics, this concept has to be questioned. We therefore studied soil denudation rates along slopes in an old-growth temperate forest that has been frequently affected by tree throw dynamics. We hypothesised that soil redistribution rates (erosion/accumulation) are easily detectable even though the landscape is dominated by a dense forest. We furthermore assumed that slope denudation driven by tree uprooting dominates over other hillslope processes under present-day conditions (cf. Šamonil et al., 2017). In this light, it would be interesting to know the extent of soil denudation rates, how they have developed over time and if tree-uprooting has always been the dominant process: we therefore tried to determine the maximum age of the 'biomantle' (Johnson, 2002) along these slopes. The increment of the root system may change the soil volume. It does, however, not actively contribute to soil denudation (Šamonil et al., 2017). This process was therefore neglected.

2 Investigation area

Europe has only very small areas having a primeval forest. Some of these areas are in the Czech Republic. The Zofinsky Primeval Forest (hereinafter Zofin) has never been cut and managed and has been under strict protection since 1838 (Šamonil et al., 2013). This area is part of the International Long-Term Ecological Research network (CZ-LTER, www.lter.cz) and the Smithsonian Institution Global Earth Observatory (SIGEO, www.sigeo.si.edu). The Zofin is close to the border of Austria (Fig. 1). The reserve extends over 102 ha (with a core zone of 50 ha) having an altitude of 730 to 837 m a.s.l. Mean annual temperature is 6.2 °C and mean annual precipitation about 866 mm. According to Tolasz et al. (2007), the average annual wind speed is 3 to 4 m s^{-1} with prevailing west wind. The average slope is 8.6°. The parent material (cover debris) consists of

granite and granodiorite (Pavlíček, 2004). The thickness of these cover debris (regolith; weathering front) is 4.6m (SD = 1.18m, max = 7.50m). The predominant soils are Cambisols, Podzols and Gleysols (IUSS Working Group WRB, 2014; Šamonil et al., 2011, 2014) with a typical thickness of about 80 cm. The analysis of a high-resolution digital elevation model (Fig. 1) showed that the western part of the Zofin area exhibits some lobes that are probably due to slow and continuous mass movement. More to the east, the topography indicates probably a high-energy mass-movement. Migoń et al. (2014) suggested that these were common activities in many mountain ranges probably during the pre-Holocene.

Pedodiversity is high on a local scale (Šamonil et al., 2011) and cannot be explained with a simple progressive soil evolution model. Old-growth forests — predominantly beech (*Fagus sylvatica* L.) with a significant proportion of spruce *(Picea abies* (L.) Karsten) and fir (*Abies alba* Mill.) — have been sporadically affected by strong storms and subsequent bark beetle (*Ips typographus* L.) outbreaks (Šamonil et al., 2013). A main soil-disturbing factor is tree uprooting. Currently, 11.65 % of the forest of the research area is covered by tree throw pit-mounds, 7.7 % of them consisting of mound areas and 4.0 % of pit areas (Šamonil et al., 2011, 2014). The tree throw rotation period is approximately 1380 years in Zofin.

3 Material and methods

3.1 General conceptual approach

Cosmogenic nuclide dating (^{10}Be) along tors and ^{10}Be in soils (Fig. 2) were used to determine long-term (millennia) soil erosion rates. Short-term (decades) rates were assessed by fallout radionuclides ($^{239+240}$Pu;) in soils. As shown by Raab et al. (2018), cosmogenic exposure dating of tors and the determination of their exhumation rates can be used to calculate surface lowering and thus soil denudation rates over millennia. Tors are large free-standing rock outcrops that are still in contact with the bedrock. Due to their higher physical resistance than the surrounding soil material, they are exhumed over time. The exhumation rate proportionally relates to the surface lowering rate and, thus, soil erosion rate (Raab et al. 2018). In addition, an average denudation rate for the

last millennia was obtained using in-situ ^{10}Be in soils.

Three main sites (Figs 1 and 2) were selected. In each of these sites, short-term soil erosion and accumulation were measured using $^{239+240}$Pu on slopes (plots 61, 173 and 177) and on a tree throw mound (plot 61). The sampling was done using small pits. An adjacent reference site (an area of about 4 x 4 m having a slope of ≈ 0°; neither at an accumulation nor at an erosion position) where no soil redistribution has occurred during the last six decades, was compared to a slope site (Table 1). At each specific site (slope positions, tree throw, reference site), four soil pit replicates were taken having 4 depth intervals (0–5, 5–10, 10–15 and 15–20cm depth) giving in total 112 samples. Soil sampling was performed using a soil corer having a volume of 100 cm^3.

The age of the slope material was estimated using the inventory of meteoric ^{10}Be in the soils (Egli et al., 2010). Similarly to $^{239+240}$Pu, the meteoric ^{10}Be stocks relate to the mass of fine earth fraction (< 2mm; its proportion was determined after sieving; see also Table 3). For this purpose, additional, large soil profiles down to the C horizon were dug at each site (slope position). We sampled each soil horizon in three randomised replicates. We also took 78 undisturbed soil samples having a volume of 100 cm^3 to determine soil density. In these same pits, in-situ ^{10}Be sampling (average denudation rate) was performed.

Soil translocation caused by tree uprooting may also affect soil aggregates. We therefore evaluated their stability to see if the formation of aggregates in the soil might have been hampered by tree uprooting processes (Walker, 2005).

The frequency of single tree throw events was calculated using tree censuses established in 1975 and repeated in 1997, 2008 and 2018 (Šamonil et al., 2017). During each census, location, health status (living standing tree, tree stump, uprooted tree etc.) of each tree (≥ 10cm in diameter at breast height DBH) and the DBH ≥ 10 cm were recorded.

3.2 Soil erosion rates determined from exposure dating of tors (^{10}Be) and ^{10}Be and $^{239+240}$Pu in soils

a) Surface lowering and soil denudation rates (^{10}Be)

The exhumation rate of tors was used as a proxy for the estimation of soil erosion rates. Tor 61 was a single rock whereas the tors at the site 177 and 177_2 were on a ridge and partly split up in different large rock pieces (Fig. 2). In this case the largest tors having no obvious signs of

exfoliation were chosen. The height-age relationship along the tor was obtained by exposure age dating the rock surface at different heights. The technique follows the principles given by Raab et al. (2018) by taking into account the age of the rock's initial appearance at the surface (subsurface ^{10}Be accumulation before exposure; t_s, equation 1).

The height–age trend along tors was modelled using different regression functions:

- a linear
- a polynomial (3rd degree) and
- a logistic function.

The logistic model is described as follows (Raab et al., 2018):

$$f(t) = \frac{a}{(1 + e^{b(t-c)})} + d \quad (1)$$

where *f(t)* corresponds to the height [m] of the sampling point along the tor, *a* is the range of height [m], *t* is time [yr], *b* is the slope coefficient [–], *c* corresponds to the time of the maximal rate of change [yr], and *d* is an asymptotic value [m]. Regression functions using Monte Carlo simulations were applied to the height-age relation by considering the external errors of the ^{10}Be measurements.

In general, the intersection of the regression function of the ages above surface with the x-axis (age) provided the age at which a tor appears at the surface. To have a better age constraint for the pre-exposure of a tor, a sample below surface was also analysed (tor 177). From height-age relationship and its mathematical derivation ($\partial f_{(t\text{-}ts)}/\partial t$), the surface lowering over time (*SL(t)*) [mm yr^{-1}] and, therefore, soil denudation rate was calculated.

$$\frac{\partial f_{(t-t_s)}}{\partial t} = SL(t) \quad (2)$$

The soil denudation rate D [t km^{-2} yr^{-1}] is defined by (Riebe et al., 2004)

$$D_{Soil} = W_{Soil} + E_{Soil} \quad (3)$$

with E_{Soil} = soil erosion and W_{Soil} = chemical weathering. In mountainous terrain, soil erosion often dominates over chemical weathering so that E_{Soil} is in the range of 0.5–0.9 × D_{soil} (Dixon and von Blanckenburg, 2012) or even higher. Thus, on slopes soil erosion is approximately

$$D_{Soil} \approx E_{soil} = SL(t) \times \rho_S \times 1000 \quad (4)$$

with ρ_s = soil bulk density [t m^{-3}].

In addition, soil denudation rates were also obtained from in-situ ^{10}Be concentrations in the topsoils (for details, see Norton et al., 2010).

b) Short-term (decades) soil erosion/accumulation rates

$^{239+240}$Pu inventories in the fine earth *As* [Bq m^{-2}] were calculated using the equation:

$$As = \frac{1}{S}\sum_i M_{Ti} C_i \quad (5)$$

where C_i = activity of the i^{th} sub-sample depth increment [Bq kg^{-1}], M_{Ti} = total mass of the i^{th} sample depth increment [kg] and S = surface area of the core [m^2]. Soil redistribution rates were then estimated by comparing an eroding/accumulating soil with a local reference inventory having no soil material redistribution. To quantify erosion/accumulation rates, the following mathematical procedures were applied:

- Profile distribution model (PDM) according to Walling and Quine (1990)
- Inventory method (IM) following Lal et al. (2013) by applying P-factors of 1, 1.2 (Walling and He 1999) and 1.5 (Lal et al. 2013).
- The code MODERN (Arata et al., 2016) was used to model the Pu-depth distribution and calculate erosion rates. MODERN usually better depicts the shape of the depth function of Pu in the soil than other models, because it does not make any assumption on the shape of the depth profile.

3.3 Soil age determination

The soil age can be estimated on the basis of meteoric ^{10}Be (e.g., Maejima et al., 2004). In accordance with procedures developed by Zollinger et al. (2017), the age is:

$$t = -\frac{1}{\lambda}\ln\left(1 - \lambda\frac{N}{q - \rho C_{10Be} f E_{soil}}\right) \quad (6)$$

where E_{soil} = soil erosion rate (in this equation as cm yr^{-1}; an average value of 0.003–0.004 cm yr^{-1} was used that corresponds to about 0.3 t ha^{-1}yr^{-1}), C_{10Be} [atoms g^{-1}] = average ^{10}Be content of the top eroding horizons, f = fine earth fraction, ρ [g cm^{-3}] = the bulk density of the top horizons, N [atoms cm^{-2}] = ^{10}Be inventory in the profile, q [atoms cm^{-2} yr^{-1}] = annual ^{10}Be deposition rate (Maejima et al., 2005), λ [4.997 x 10^{-7} yr^{-1}] = decay constant of ^{10}Be and t [yr] = surface age.

3.4. Estimation of soil redistribution rates using tree throw census data

The average amount of soil made available for denudation by tree throws was estimated based on (i) the detailed knowledge of single uprooting events in the forest reserve between 1975 and 2018 from repeated censuses of circa 24000 trees having a DBH ≥ 10 cm in an area of 74.2 ha (Průša, 1985), (ii) slope angle on site, (iii) the deviation of tree fall direction from downslope direction, and (iv) the modelled relationship between tree DBH and root plate volume (Šamonil et al., 2017).

First, a general model of the proportion of material that settles back into the tree throw pit as the mound erodes was created. This approach is based on a hydraulic erosion simulation algorithm after Mei et al. (2007) and Šťáva et al. (2008). We used an experience-based idealised representation of a pit-mound microtopography consisting of two half-ellipsoids of equal volume and width. While the pit ellipsoid had a circular projection (length same as width) the length of the mound half-ellipsoid has half its width. We ran the algorithm for 49 different combinations of inclination (0–60°) and tree fall direction (0–180° deviation from downslope direction) and fitted a linear model to these results (R^2=0.999) to predict the proportion of material returning to the pit for any combination of the two parameters. In a next step, we computed for every tree uprooted between 1975 and 2008 its tree throw mound volume using the following equation (Šamonil et al. 2017):

$$V = 0.001313\ DBH^2 \quad (7)$$

where V = tree throw root plate volume [m^3]. Based on the slope inclination and fall direction of the tree trunk, the volume of soil that would not return back to the pit was estimated. Finally, these volumes were used to estimate the average annual contribution of tree throw dynamics to denudation rates for different inter-census periods.

Charcoal fragments in the soils documented the presence of a forest for the last 11 kyr (Bobek et al., 2018).

3.5 Analytical procedure

Surface exposure dating:

About 2 kg of rock material was taken per sample (tor and rocks) with a stone saw, hammer and

chisel. The shielding factor was determined in the field using a Suunto inclinometer. The rock samples were subsequently crushed and sieved to the fraction 0.5–1 mm. Feldspar was removed by froth flotation. In a subsequent step, the samples were leached for one week with hydrofluoric acid (HF) in a shaker to obtain pure quartz. The procedure to extract $Be(OH)_2$ and its calcination is described in detail in Dahms et al. (2018). All $^{10}Be/^{9}Be$ ratios were measured at the ETH Zurich AMS system Tandy (Christl et al., 2013) and normalised to the ETH Zurich in-house AMS standard S2007N ($^{10}Be/Be$ = 28.1 x 10^{-12} nominal) which has been calibrated relative to ICN 01-5-1 ($^{10}Be/^{9}Be$ = 2.709 x 10-11 nominal) (Nishiizumi et al., 2007) — both associated with a ^{10}Be half-life of 1.387±0.012 My (Chmeleff et al., 2010). ^{10}Be contents were blank corrected. ^{10}Be exposure ages were calculated using CRONUS-Earth (http://hess.ess.washington.edu/math/) version 3.0 (Table S1). The production rate, and thus the age, was corrected for latitude and altitude using the time-dependent (Lal/Stone) scaling scheme (Lal, 1991; Stone, 2000).

In-situ ^{10}Be in soils:

At each site (61, 173, 177) about 5–6 kg of soils were sampled from the top 50 cm. After drying, the samples were sieved to 250–500 µm and quartz was extracted via standard physical and chemical separation. An in-house ^{9}Be carrier was added and Be was extracted at the Victoria University of Wellington Cosmogenic Nuclide Lab following Norton et al. (2010). Erosion rates were calculated using CRONUS-Earth version 3.0.

Meteoric ^{10}Be:

The stocks of meteoric ^{10}Be were measured using the fine earth (fraction ≤ 2 mm) of each soil horizon of the three soil profiles (no. 61, 173, 177) as described in Zollinger et al. (2017). Meteoric ^{10}Be was extracted from the soil material according to Egli et al., 2010 (and references therein). The $^{10}Be/^{9}Be$ ratios were measured at the ETH Zurich AMS system Tandy as previously described and blank corrected.

$^{239+240}Pu$:

Fallout radionuclides (e.g. $^{239+240}$Pu) are a product of above-ground nuclear weapons testing and were emitted to the upper atmosphere particularly during the 1950–1960's and/or by nuclear reactor accidents. Scavenged by rain or by dry deposition, Pu strongly binds to the soil. Transuranic elements, such as Pu, are mainly found in surficial soils and the entire stock is found in the top 20 or 30 cm (Ketter et al., 2011).

Sample preparation was done following Ketterer M.E., Szechenyi (2008) . The finely milled samples were ashed for 20 h (600 °C) to remove organic matter. A spike of c. 30 picograms (0.0044 Bq) of ^{242}Pu tracer solution (NIST 4334) was added. The samples were then leached and Pu species adjusted to a Pu^{4+} oxidation state. After heating at 75 °C, TEVA resin was added. After rinsing, Pu was eluted and was ready for analysis. Together with the samples, pre-bomb soils ('negative control'), the Standard Reference Material 4350b (river sediment, NIST) and blanks were analysed. The Pu activity of soil samples is reported in Table S2.

The Pu isotopes were measured using an Agilent 8800 Triple QQQ-ICP-MS (APEX HF, ESI Scientific, Omaha, NE, USA).

Soil aggregates:

Soil aggregates were determined according to Nimmo and Perkiins (2002) by using sieves having mesh sizes of 1, 0.5, 0.25 and 0.125 mm. The mean weight diameter (MWD) of all size classes from dry and wet sieving (> 5 mm down to < 125 µm) was determined

$$MWD_i = \frac{\sum m_{wi} \times \overline{d_i}}{\sum m_i}; \qquad MWD = \sum MWD_i \tag{8}$$

with MWD_i = mean weight diameter of the "i-th" sieve class, m_{wi} = sum of the mass fraction of soil remaining on each sieve after sieving [g], d_i = the mean mesh size of the "i-th" sieve [mm] and m_i = the total amount [g] of used sample weight (Nimmo and Perkiins, 2002).

Additionally, we calculated the MWD using the equation of Chenu et al. (2011):

$$MWD = 0.34\, C_{org} + 0.008\, clay + environment \tag{9}$$

The factor 'environment' has a value of -0.17 for grassland and 0.34 for forests.

Geochemistry of the soils:

The total element content was determined in powder samples using X-ray fluorescence (SPECTRO X-LAB 2000). Soil pH (H_2O) was measured in a soil:solution ratio of 1:2.5. Fe, Al and Si concentrations were determined (in duplicate) after treatment of the soil samples with NH_4-oxalate (buffered at pH 3; McKeague et al., 1971) and dithionite (only Fe and Al; Borggaard, 1988). Subsequently, the element contents were analysed using atomic absorption spectroscopy. The total organic carbon (C) and nitrogen (N) contents were determined using isotope ratio mass spectrometry (IRMS).

4 Results

4.1. Characteristics of the soil profiles

Profile 61 (Dystric Cambisol; Table 1) is located on a midslope position and has a thickness of c. 80 cm (Table 2). The soil is acidic, has a high organic C content in the topsoil and exhibits a high amount of pedogenic forms of Fe and Al in the upper part of the profile. The dithionite-extraction usually determines amorphous and crystalline Al- and Fe-oxyhydroxides, including also organically bound Fe and Al in a soil (Borggaard, 1988). With oxalate, non-crystalline and weakly crystalline forms are extracted. The oxalate-extractable Al content is slightly higher than the dithionite-extractable content, indicating that no crystalline Al-forms are present. An active formation of imogolite type materials (ITM) does not take place because the molar Al/Si ratios are far outside the range 1–2 (Parfitt and Hemni, 1982). The other two profiles (173 and 177) have both spodic characteristics and are thicker with a genetic depth of about 100 cm. Profile 173 is located at the footslope and shows the typical eluviation and illuviation of organo-metallic complexes in an Albic Podzol. The spodic characteristics are less pronounced in profile 177 (Entic Podzol).

4.2. Tor exposure ages and denudation rates

Along tor 61, the exposure age constantly increased from 16 ka close to the soil surface up to 67 ka at 1.8 m height (Fig. 3). The ^{10}Be content at the rock surface increases with tor height. This reflects our basic assumption that tors are exhumed over time and exposed to atmosphere.

Although almost linear, the age trend can be best modelled using a polynomial function (Fig. 4a-c). The R^2 obtained using a linear regression were significantly lower than when using a polynomial function. The logistic function (equation 9) does neither differ from the linear nor from the polynomial approach. Taking the pre-exposure of the rock into account, the tor represents exhumation rates and thus surface lowering rates over the last c. 51 kyr. The average exhumation rates are about 0.032 mm yr^{-1}. Assuming an average soil bulk density of c. 0.9 t m^{-3}, then soil denudation rate is roughly 30 t km^{-2} yr^{-1}. Using the derivation of the polynomial function, the calculated rates would show a maximum around c. 10–30 kyr with about 30–50 t km^{-2} yr^{-1} (Fig. 4g) that are slightly decreasing in the Holocene to about 20–30 t km^{-2} yr^{-1}. Very low erosion rates seemed to have prevailed during the last glacial period.

Tor 177 gave an increase in age with height above surface while the contrary was the case for tor 177_2 (another tor in close vicinity to tor 177). The average slope (change of age as a function of height) is for all tors very similar (Fig. 3). Due to the contrary age trend of tor 177_2, we have to assume that this 'tor' toppled over. While resampling this tor (backside) we recognised that, from a morphological point of view, something must have happened to this rock (confirmed by an additional age that does not fit into the trend; Table 3). The relatively good age resolution along tor 177 enabled the determination of exhumation rates over time and, thus, indirectly soil erosion rates over time. The surface ages and external errors were used for a trend fitting (height vs. age; Fig. 4d–e). Compared to the other approaches, the logistic model gave for tor 177 clearly the best results ($p < 0.01$) when tracing the height-age trend. The linear model does not adequately represent this trend. Furthermore, it was not possible to model the trend in a meaningful way when using a polynomial approach without fixing (arbitrarily) some parameters (e.g. intersection with the x-axis, ignoring negative trends). As a consequence, polynomial functions were not further considered in this case. Using this approach, a maximum value of surface lowering rates (soil erosion rates) can be determined for the transition period between the Pleistocene and Holocene. During a large part of the last ice age, the soil erosion rates probably seemed to be very low. After the erosion peak at the Pleistocene/Holocene transition (mean value: about 75 t km^{-2} yr^{-1} and having a range of about 58–91 t km^{-2} yr^{-1}, Fig. 4f), the erosion rates remained at a distinctly higher level than before the peak. According to this time trend model (Fig. 4f), the present-day net erosion

rates are in the range of 35–72 t km^{-2} yr^{-1}. The average surface lowering rate over the entire period is 0.04 mm yr^{-1} or, in terms of soil denudation, about 40 t km^{-2} yr^{-1}.

Assuming that tor 177_2 toppled over, an exhumation rate can be calculated. The slope of the age trend is, although negative, similar to the other tors. By multiplying this age trend with a factor -1, the average exhumation rate would have been 0.023 mm yr^{-1} corresponding to an average erosion rate of 23 t km^{-2} yr^{-1}. This value has however to be considered with caution.

The in-situ ^{10}Be denudation rates (soils) are, in average, significantly faster with 58–76 t km^{-2} yr^{-1}, perhaps supporting enhanced tree throw during the Holocene (Table 4).

4.3. Short-term denudation rates using $^{239+240}$Pu

Nuclear fallout radionuclides. such as Pu, can be used as tracer for soil erosion rates for the last five to six decades (Meusburger et al., 2016). Pu was concentrated in the topmost 5 cm of the soils and exponentially decreased with depth (Fig. 5).

Soil erosion was detectable at the plots 61 and 173 (Table 4). The tree uprooting site (mound) erodes quickly. In contrast to our expectance, no erosion was measured at site 177 but instead accumulation occurred. Depending on the calculation procedure, the erosion rates vary slightly (Table 4). Independent of the calculation procedure, the erosion rates are highest at the tree uprooting site. Although the tree was already rotten and thus tree uprooting must have occurred probably more than 50 years ago (Šebková et al., 2012; Petrillo et al., 2016), slope activity is still highest.

The short-term soil redistribution rates seem higher than the long-term rates (^{10}Be). If, however, the average short-term values of all sites (Table 4) are calculated (42 to 77 t km^{-2} yr^{-1}) then these rates are similar to the long-term rates and even closer to the rates obtained for the Holocene when using ^{10}Be (along tors and in soils).

4.4 Soil aggregate stability

The MWD values did not vary greatly and were for all three profiles approximately 2 (Table 5). The MWD values using the equation of Chenu et al. (2011), differ slightly from the measured MWD values. The highest difference is found in profile 177. This can be explained by the high C content

in the Ah horizon of this profile. When comparing the MWD values to the classes of Le Bissonnais (1996), then the soil aggregates of all profiles can be characterised as stable to very stable.

4.5. Meteoric ^{10}Be in the soils and age estimation

In all soils, a relatively low ^{10}Be concentration was measured in the uppermost soil horizon (Fig. 6). This could be due to (i) leaching of ^{10}Be from this horizon to greater depths or (ii) mechanical soil disturbance (e.g. tree uprooting). At plot 173, the ^{10}Be trend with depth seems to follow podzolisation, i. e. eluviation of organo-metallic complexes from the uppermost A and E horizons and their illuviation and precipitation in the spodic Bhs and Bs horizons (Sauer et al. 2007). A part of ^{10}Be migrated to these horizons beneath. At plot 61 (Fig. 6), the zigzag of ^{10}Be along the profile is unusual and indicates a redistribution of soil material most probably by one or several tree uprootings that occurred hundreds or thousands of years ago (Šamonil et al., 2013). However, redistribution was not obvious when having a look at the pedomorphic properties, thus, suggesting very old disturbance events. Podzolisation is not that intense in profile 177. The low ^{10}Be concentrations probably are due to a vertical translocation and accumulation of uprooted material.

To calculate soil age or the residence time of the soil material, the stock of ^{10}Be and the deposition rates must be known. Average concentrations of ^{10}Be in rainfall are near 1–1.5 × 10^4 atoms cm^{-3} (Heikkilä et al., 2008; Graly et al., 2011). Multiplying the ^{10}Be content in rainfall with the annual precipitation gives the input of ^{10}Be. However, annual precipitation rates are not precisely known for very long periods (millennia). Assuming that the present-day's average of annual precipitation more-or-less matches the average of the Holocene, then an estimate for this period can be made. The investigated soils are older and already started to form in the Pleistocene. For this period, only imprecise estimates based on existing glaciological and palaeoclimatological investigations can be made. According to Heyman et al. (2013), annual precipitation was during the last glacial maximum probably 25–75% of the present-day situation. We made a scenario calculation by taking these values iteratively into account by using:

$$P = P_H \times F + P_{IA} \times (1 - F) \quad (10)$$

where P = precipitation rate [mm yr^{-1}] during entire period of soil formation, P_H = precipitation rate during the Holocene, F = precipitation proportionality factor (ratio time of soil evolution during the

Holocene to entire duration of soil formation) and P_{IA} = precipitation rate during the Pleistocene (25–75 % of present-days rate). In addition, the approximate average erosion rate was used that was calculated from the exhumation rate of the tors (c. 30 t km^{-2} yr^{-1}). Using this approach, the age range of soil profile 61 is approximately between 60 and 150 ka, profile 173 between 21 and 45 ka and profile 177 between 50 and 110 ka (Fig. 7). In these calculations, erosion and thus surface lowering is implemented (equation 6). As a consequence, soil can be considered as a flow-through reactor of the top about 0.8–1 m (see discussion chapter).

4.6. Contribution of tree throw dynamics to denudation rate

The average annual transport of soil material due to tree uprooting was 3.5 m^3 ha^{-1} yr^{-1} between 1975 and 2018 (Table 7; tree throw census data). Although the majority of the moved soil returns back to the tree throw pit during the post-disturbance erosion-sedimentation process (considering the slope angle and the direction of tree fall, Fig. 8), about 1.5 m^3 of soil per hectare and year (i.e. 150 t km^{-2} yr^{-1}; Table 7) continued to move downslope and may have contributed to slope denudation. However, an exceptionally disturbing event with a return interval of c. one century (Šamonil et al., 2013) occurred during the monitoring period influencing these average values. Considering one strong storm per century (e.g. Kyrill storm in January 2007), the tree throw net denudation rates are about 92 t km^{-2} yr^{-1} (computed as a weighted average by reducing the proportion of the Kyrill-containg period 1997-2008 to the whole observation period). An unknown part of the translocated material by tree uprooting along the slope is redeposited. This means that the net soil erosion rate due to tree uprooting is actually lower than 150 t km^{-2} yr^{-1} and in the long term even lower than 92 t km^{-2} yr^{-1} (these values represent maximum rates).

5 Discussion

5.1. Long-term evolution of erosion rates (using ^{10}Be)

The obtained average, long-term denudation rates (^{10}Be) of c. 30 t km^{-2} yr^{-1} are low, but seem reasonable for forested and natural sites that are not on steep slopes and agree well with literature data (Morgan, 1999; Pieri, 1992). The long-term denudation rates derived from ^{10}Be in the soils

(quartz) are with 58–76 t km^{-2} yr^{-1} slightly higher, but still at a low level.

The investigated tor 177 exhibits a maximum of erosion rates about 10 –15 ka (transition period: Pleistocene – Holocene). This trend would nicely fit to findings of Raab et al. (2018) who measured distinctly increased erosion rates (up to about 150–300 t km^{-2} yr^{-1}, compared to rates that were usually < 20 t km^{-2} yr^{-1}). Therefore, the measured increase in denudation/erosion (up to 58–91 t km^{-2} yr^{-1}) around 10–15 ka ago in the Zofin area might be due to the drastic climate change that occurred at the transition from the Pleistocene to the Holocene. Also the second tor (61) indicates a maximum of erosion rates between about 10–30 ka. However, the signal derived from this tor is slightly speculative, because the exhumation trend can also be well explained using a linear trend (with no rate changes over time) and the obtained erosion peak is very broad. To have more conclusive results about the temporal evolution of denudation rates over time, more tors would need to be sampled and analysed. Our hypothesis of an increased erosion activity during the transition from the Pleistocene to the Holocene is further supported by findings of Migoń et al. (2014) who found that high-energy mass-movements were common in many mountain ranges in these areas before the onset of the Holocene whereas during the Holocene such processes are not that evident anymore and soil formation prevails.

According to Raab et al. (2018), erosion rates show a fluctuation over time that is related to major climate changes. These authors calculated maximum erosion rates during such transition times in the range of about 150–300 t km^{-2} yr^{-1} for a Mediterranean upland. The variations depend on local conditions: in the Appalachian, for example, the late Pleistocene was a period having intense erosion. With Holocene warming, periglacial processes stopped and erosion decreased (Mills and Delcourt, 1991; Montgomery and Wohl, 2004). Erosion rates can be high until a vegetation cover or forest is established. About 11 ka BP (Bobek et al., 2018), a forest-like vegetation must have already existed in the Zofin area. With changing climate, the sparse vegetation before 11 ka BP gave way to *Pinus sylvestris*/*mugo* forests with frequent forest fires between 11–9 ka BP that probably have enhanced soil erosion. Once *Fagus sylvatica* established, fire frequency decreased. Bobek et al. (2018) found fire disturbances until about 6 ka BP. Because fire events generally decrease the frequency of tree uprootings (Schaetzl and Thompson 2015), the volume of the tree throw soil redistribution rates (0.92 m^3 ha^{-1} yr^{-1}) must have been lower before 6 ka BP. After 9 ka,

rapid climate deterioration phases existed that have enhanced soil erosion (e.g. around 8.4 ka, Malkiewicz et al., 2016).

5.2. Recent erosion rates (using $^{239+240}$Pu and tree censuses)

The short-term erosion values revealed by Pu isotopes are untypically high for forests. Usually, very low values or even no erosion is surmised for forested areas (Meusburger and Alewell, 2014). However, Meusburger et al. (2013) were able to measure high soil erosion rates even in forested and monsoon affected areas having steep steep slopes using ^{137}Cs and RUSLE (South Korea; with erosion rate between 2 – 700 t km^{-2} yr^{-1}). The present-day erosion rates in the Zofin area are locally 50 to > 100 t km^{-2} yr^{-1}. These values fit nicely with the modelled values from tree uprooting monitoring (average = 92 t km^{-2} yr^{-1}). Three different models were used to calculate erosion rates based on $^{239+240}$Pu. In contrast to Meusburger et al.'s (2016) findings, the results seem comparable independent of the modelling approach (Fig. 9).

Tree uprooting redistributes soil material leading to both, erosion and accumulation. If the mean value of the obtained erosion/accumulation rates using Pu (without the mound at the TUR site; Table 4) of soils is calculated, then we obtain a net denudation in the range of 17–37 t km^{-2} yr^{-1}; with the TUR site the range is 42–77 t km^{-2} yr^{-1}. These values fit well to the determined rates derived from the exhumation rate of the tors and ^{10}Be in soils.

Although tree-uprooting gives rise to soil redistribution soil aggregates are stable which is typical for forest soils (Chenu et al., 2011). This again indicates that erosion is not continuous but rather episodic and that longer phases with stable conditions occur.

The biomechanical effects of trees is highest at altitudes between 700–1200 m a.s.l. in central European temperate and native forest (Šamonil et al., 2017) which seems to be due to the size of trees (that normally decreases with altitude) and number of storm events. The calculated net erosion rates based on tree censuses are probably slightly too high (92 t km^{-2} yr^{-1}). Using the Pu-isotopes, we measured similar values only on mounds. Pawlik (2013) estimated in a review paper biogenic creep globally in the range of 20 to 130 t km^{-2} yr^{-1}.

Since soil redistribution due to tree uprooting is patchy, it is expected that disturbed sites have higher rates than currently undisturbed areas. While rare strong storms increase the denudation

effect of tree uprootings, the absence of storm events or a too-high frequency limit the biogeomorphic effect of trees (Constantine et al., 2012). We assume that the current disturbance regime, climate and soil conditions favour the biogeomorphic effect of trees.

5.3 Meteoric ^{10}Be in the soil

Meteoric ^{10}Be may take part in pedogenic processes, such as eluviation/illuviation-related distributions, that imposes difficulties when dating soils (Wyshnytzky et al., 2015). Some authors (Egli et al., 2010; Waroszewski et al., 2018) found a positive correlation between ^{10}Be and oxalate-extractable Fe or Al and sometimes C_{org} in Podzols. From these relationships, these authors postulated a downward migration of ^{10}Be together with Fe, Al and/or organic matter. Other authors however state that ^{10}Be does not show consistent trends in hillslope soils (Wyshnytzky et al., 2015). Graly et al (2010) observed a correlation between ^{10}Be and dithionite-extractable Al and clay but no or only a weak correlation to dithionite-extractable Fe. It is therefore difficult to draw a general pattern between ^{10}Be and soil characteristics. ^{10}Be in the investigated soils did not show any correlation to almost any of the previously mentioned parameters. Only in the profiles 173 and 177, a correlation was found between ^{10}Be and oxalate and dithionite-extractable Al. This suggests that ^{10}Be is partially involved in podzolisation.

When dating soils using meteoric ^{10}Be, the estimation of ^{10}Be deposition rates for a specific site is the most error-prone step (Egli et al., 2010). Only an estimate of ^{10}Be deposition rates can be provided for these long periods. Soils in temperate to alpine regions seem to attain a steady state after about 100 ka (Egli et al., 2018) or even earlier and often reach a thickness of about 0.8–1m. Yu et al. (2017) and Egli et al. (2018) gave the physical explanation for this phenomenon. Consequently, the investigated soils are close to a quasi steady-state because the area was not glaciated during the last glaciation (Heyman et al., 2013) and soil formation must have started > 100 ka; except major landsliding or other events would have occurred leading to a resetting. In a quasi-steady-state, the determined soil ages (Fig. 7) indicate a mean residence time of a particle in the previously mentioned soil layer. Assuming a long-term erosion rate of 0.3 t ha^{-1} yr^{-1} at quasi-steady-state conditions and a bulk density of the whole soil of approximately 0.9 t m^{-3}, then the mean residence time would be about 45 kyr for a soil having a thickness of 1.5 m and 30 kyr for a

soil having a thickness of 1m which is in the range of the determined ^{10}Be soil ages. Probably all soils have a similar age, but evolved differently due to different topographic positions, moisture conditions and biogenic creep.

6 Conclusions

^{10}Be exposure ages along tors enabled the construction of a model for soil erosion rates during the last c. 50–70 kyr. The model derived from one tor shows that an erosion rate of about 75 t km^{-2} yr^{-1} (range between 58–91 t km^{-2} yr^{-1}) has occurred at the transition from the Pleistocene to the Holocene owing to a strong climate change. When using this model, the present-day net erosion rates are in the range of 35–72 t km^{-2} yr^{-1}. These are high values when compared to rates of the pre-LGM (Last Glacial Maximum). However, another analysed tor did not provide such a clear temporal trend. Therefore, the previously mentioned maximum at the transition from the Holocene to the Pleistocene remains slightly speculative.

The long-term denudation rates derived from ^{10}Be in the soils (quartz) give an average for the last few millennia in the range of 58–76 t km^{-2} yr^{-1}. Using $^{239+240}$Pu as a tracer, the present-day erosion rates on mounds locally reached 100 to 200 t km^{-2} yr^{-1} due to tree uprooting. Uprooting itself induces strong denudation processes with erosion on the mound and infilling in the pits. If the average of erosion and accumulation is calculated, then a net denudation rate in the range of 16–77 t km^{-2} yr^{-1} was obtained that fits to the determined long-term values derived from the exhumation rate of the tors. The tree throw census indicates that large volumes have been involved in soil redistribution. Based on this inventory, the denudation rates are max. 92 t km^{-2} yr^{-1}. Both applied indexes indicate stable soil aggregates conditions and show typical values for forests. This again demonstrates that erosion is not continuous and that longer periods with stable conditions exist.

The multi-method approach shows that biogenic creep (tree uprooting) contributes significantly to the overall denudation and is probably the most important factor for the last few thousands of years in such environments.

Acknowledgements This research was supported by the Czech Science Foundation (project no. 19-09427S). Kevin Norton had a Rutherford Discovery Fellowship from the Royal Society Te Apārangi. The authors thank the colleagues of the Blue Cat research team for their help with data collection. We are furthermore indebted to three unknown reviewers and Tony Reimann for their helpful and constructive comments.

References

Arata, L., Meusburger, K., Frenkel, E., A'Campo-Neuen, A., Iurian, A.-R., Ketterer, M.E., Mabit L, & Alewell, C. (2016). Modelling Deposition and Erosion rates with RadioNuclides (MODERN) – Part 1: a new conversion model to derive soil redistribution rates from inventories of fallout radionuclides. *Journal of Environmental Radioactivity, 162–163,* 45–55. doi:10.1016/j.jenvrad.2016.05.008

Balco, G., Stone, J.O., Lifton, N.A., & Dunai, T.J. (2008). A complete and easily accessible means of calculating surface exposure ages or erosion rates from ^{10}Be and ^{26}Al measurements. *Quaternary Geochronology, 8,* 174-195. DOI: 10.1016/j.quageo.2007.12.001

Bobek, P., Šamonil, P., & Jamrichová, E. (2018). Biotic controls on Holocene fire frequency in a temperate mountain forest, Czech Republic. *Journal of Quaternary Science*, *33,* 892–904. doi:10.1002/jqs.3067

Borggaard, O. K. (1988). *Phase indication by selective dissolution techniques.* In: Iron in Soils and Clay Minerals, Stucki, J. W., Goodman, B. A., Schwertmann, U. (eds). D. Reidel: Dordrecht, 83–89. doi:10.1007/978-94-009-4007-9_5

Bormann, B.T., Spaltenstein, H., McCleellan, M.H., Ugolini, F.C., Cromack Jr., K., & Nay, S.M. (1995). Rapid soil development after windthrow disturbance in pristine forests. *Journal of Ecology*, *83*, 747**–**757. DOI: 10.2307/2261411

Chmeleff, J., von Blanckenburg, F., Kossert, K., & Jakob, D. (2010). *Determination of the ^{10}Be half-life by multicollector ICP-MS and liquid scintillation counting.* Nuclear Instruments and Methods in Physics Research Section B: Bean Interaction with Materials and Atoms 268, 192-199. DOI: 10.1016/j.nimb.2009.09.012

Chenu, C., Abiven, S., Annabi, M., Barray, S., Bertrand, M., Bureau, F., Cosentino, D., Darboux, F.,

Duval, O., Fourrié, L., Francou, C., Houot, S., Jolivet, C., Laval, K., Le Bissonnais, Y., Lemée, L., Menasseri, S., Pétraud, J. P., & Verbèque, B. (2011). Mise au point d'outils de prévision de l'évolution de la stabilité de la structure de sols sous l'effet de la gestion organique des sols. *Etude et Gestion des Sols*, 18, 161–174. doi: 10.5167/uzh-51361

Christl, M., Vockenhguber, C., Kubik, P.Q., Wacker, L., Lachner, J., Alfimov, V., & Synal, H.A. (2013). *The ETH Zurich AMS facilities: Performance parameters and reference materials.* Nuclear Instruments and Methods in Physics Research B 294: 29-38. doi: 10.1016/j.nimb.2012.03.004

Cizdziel, J.L., Ketterer, M.E., Farmer, D., Faller, S.H., Hodge, V.F. (2008). $^{239,\ 240,\ 241}$Pu fingerprinting of plutonium in western US soils using ICPMS: solution and laser ablation measurements. *Anal Bioanal Chem*, *390*, 521**–**530. DOI 10.1007/s00216-007-1741-x

Constantine, J. A., Schelhaas, M. - J., Gabet, E. & Mudd, S. M. (2012). Limits of windthrow-driven hillslope sediment flux due to varying storm frequency and intensity. *Geomorphology, 175–176*, 66–73. doi:10.1016/j.geomorph.2012.06.022

Dahms, D., Egli, M., Fabel, D., Harbor, J., Brandová, D., Portes R., & Christl, M. (2018). Revised Quaternary glacial succession and post-LGM recession, southern Wind River Range, Wyoming, USA. *Quaternary Science Reviews, 192,* 167–184. doi: 10.1016/j.quascirev.2018.05.020

Dixon, J. L., & von Blanckenburg, F. (2012). Soils as pacemakers and limiters of global silicate weathering. *Comptes Rendus Geoscience*, *344*, 597–609. doi:10.1016/j.crte.2012.10.012

Egli, M., Brandová, D., Böhlert, R. Favilli, F., & Kubik, P. (2010). ^{10}Be inventories in Alpine soils and their potential for dating land surfaces. *Geomorphology*, *119*, 62–73. doi.10.1016/j.geomorph.2010.02.019

Egli, M., Hunt, A., Dahms, D., Raab, G., Derungs, C., Raimondi, S., & Fang, Y. (2018). Prediction of soil formation as a function of age using the percolation theory approach. *Frontiers in Environmental Science, 6,* 108, doi: 10.3389/fenvs.2018.00108.

Gabet, J. E., & Mudd, S. M. (2010). Bedrock erosion by root fracture and treethrow: a coupled biogeomorphic model to explore the humped soil production function and the persistence of hillslope soils. *Journal of Geophysical Research*, *115*, F04005. doi:10.1029/2009JF001526

Graly, J.A., Bierman, P.R., Reusser, L.J., Pavich, M.J. (2010). Meteoric ^{10}Be in soil profiles — A global meta-analysis. *Geochimica et Cosmochimica Acta*, 74, 6814-6829. doi:10.1016/j.gca.2010.08.036

Graly, J. A., Reusser, L. J., & Bierman, P. R. (2011). Short and long-term delivery rates of meteoric ^{10}Be to terrestrial soils. *Earth and Planetary Science Letters*, *302*, 329–336. doi:10.1016/j.epsl.2010.12.020

He, Q., & Walling, D. E. (1997). The distribution of fallout ^{137}Cs and ^{210}Pb in undisturbed and cultivated soils. *Applied Radiation and Isotopes*, *48*, 677–690. doi:10.1016/S0969-8043(96)00302-8

Heikkilä, U., Beer, J., & Alfimov, V. (2008). Beryllium-10 and beryllium-7 in precipitation in Dübendorf (440 m) and at Jungfraujoch (3580 m), Switzerland (1998–2005). *Journal of Geophysical Research*, *113*, D11104. doi:10.1029/2007JD009160

Heyman, B. M., Heyman, J., Fickert, T., & Harbor, J. M. (2013). Paleo-climate of the central European uplands during the last glacial maximum based on glacier mass-balance modelling. *Quaternary Research*, *79*, 49–54. doi:10.1016/j.yqres.2012.09.005

IUSS Working Group WRB. (2014). *World Reference Base for Soil Resources 2014*. World Soil Resources Reports No. 106. FAO, Rome.

Johnson, D. L. (2002). Darwin would be proud: bioturbation, dynamic denudation, and the power of theory in science. *Geoarchaeology*, *17*, 7–40. doi: 10.1002/gea.10001

Johnson, D.L. & Watson-Stegner, D. (1987). *Evolution model of pedogenesis. Soil Science 143*: 349–366.

Johnson, D.L., Domier, J.E.J. & Johnosn, D.N. (2005). Animating the biodynamics of soil thickness using process vector analysis: a dynamic denudation approach to soil formation. *Geomorphology, 67*, 23-46. https://doi.org/10.1016/j.geomorph.2004.08.014

Ketterer M.E., Szechenyi S.C. (2008). Determination of plutonium and other transuranic elements by inductively coupled plasma mass spectrometry: a historical perspective and new frontiers in the environmental sciences. *Spectrochim. Acta Part B.* 63, 719–737. https://doi.org/10.1016/j.sab.2008.04.018

Ketterer, M., Zheng, J., & Yamada, M., (2011). Applications of transuranics as tracers and

chronometers in the environment. In: M. Baskaran (ed.), *Handbook of Environmental Isotope Geochemistry,* Advances in Isotope Geochemistry, , # Springer-Verlag Berlin Heidelberg 2011, pp. 395-417, DOI 10.1007/978-3-642-10637-8_20

Kirkby, M.J. (1967). Measurement and theory of soil creep. *The Journal of Geology*, *75*, 359–378. www.jstor.org/stable/30085000.

Kirkby, M. J. (2004). *Soil creep*. In: Goudie, A. S. (Ed.), Encyclopedia of Geomorphology. Routledge, London and New York, 974–977.

Lal, D. (1991). Cosmic ray labeling of erosion surfaces: in situ nuclide production rates and erosion models. *Earth and Planetary Science Letters*, *104*, 424–439. doi:10.1016/0012-821X(91)90220-C

Lal, R., Tims, S. G., Fifield, L. K., Wasson, R. J., & Howe, D. (2013). Applicability of 239Pu as a tracer for soil erosion in the wet-dry tropics of northern Australia. Nuclear instruments and *Methods in Physics Research Section B Beam Interactions with Materials and Atoms*, *294*, 577–583. doi:10.1016/j.nimb.2012.07.041

Le Bissonnais, Y. (1996). Aggregate stability and assessment of soil crustability and erodibility: I. Theory and methodology. *European Journal of Soil Science*, *47*, 425–437.

Lehre, A. K. (1987). Rates of soil creep on colluvium-mantled hillslopes in north-central California. In: Beschta, R., Blinn, T., Grant, C., Ice, G., Swanson, F. (Eds.), *Erosion and sedimentation in the Pacific Rim*. IAHS Press, Wallingford, 165, 91–100. https://doi.org/10.1111/ejss.2_12311|

Mei, X., Decaudin, P., & Hu, B. G. (2007). Fast hydraulic erosion simulation and visualization on GPU. *15th Pacific Conference on Computer Graphics and Applications*, PG '07, Maui, United States, pp. 47–56. 10.1109/PG.2007.15

Maejima, Y., Matsuzaki, H., & Nakano, C. (2004). ^{10}Be concentrations of red soils in Southwest Japan and its possibility of dating. *Nuclear Instruments and Methods in Physics Research B 223–224*, 596–600. doi:10.1016/j.nimb.2004.04.110

Maejima, Y., Matsuzaki, H., & Higashi, T. (2005). Application of cosmogenic ^{10}Be to dating soils on the raised coral reef terraces of Kikai Island, southwest Japan. *Geoderma*, *126*, 389–399. doi:10.1016/j.geoderma.2004.10.004

Malkiewicz, M., Waroszewski, J., Bojko, O., Egli, M., & Kabala, C. (2016). Holocene vegetation history and soil development reflected in the lake sediments of the Karkonosze Mountains (Poland). *The Holocene*, *26*, 890-905. DOI: 10.1177/0959683615622546

McKeague, J. A., Brydon, J. E., & Miles, N. M. (1971). Differentiation of forms of extractable iron and aluminium in soils. *Soil Science Society of America Proceedings*, *35*, 33–38. doi:10.2136/sssaj1971.03615995003500010016x

Meusburger K., Mabit L., Park J.H., Sandor T., & Alewell C. (2013). Combined use of stable isotopes and fallout radionuclides as soil erosion indicators in a forested mountain site, South Korea. *Biogeosciences*, 10, 5627–5638. 10.5194/bg-10–5627–2013.

Meusburger K., & Alewell C. (2014). *Soil Erosion in the Alps. Experience gained from case studies (2006–2013)*. Federal Office for the Environment, Bern. Environmental studies no. 1408: 116 pp.

Meusburger, K., Mabit, L., Ketterer, M., Park, J. H., Sandor, T., Porto, P., & Alewell, C. (2016). A multi-radionuclide approach to evaluate the suitability of $^{239+240}$Pu as soil erosion tracer. *Science of the Total Environment*, 566, 1489–1499. doi:10.1016/j.scitotenv.2016.06.035

Migoń, P., Kacprzak, A., Malik, I., Kasprzak, M., Owczarek, P., Wistuba, M., & Pánek, T. (2014). Geomorphological, pedological and dendrochronological signatures of a relict landslide terrain, Mt Garbatka (Kamienne Mts), WS Poland. *Geomorphology, 2019*, 213-231. http://dx.doi.org/10.1016/j.geomorph.2014.05.005

Mills, H.H., & Delcourt, P.A. (1991). Quaternary geology of the Appalachian Highlands and Interior Plateaus. In: *Quaternary Nonglacial Geology*. Conterminous U.S. Geological Society of America, Boulder, CO, pp. 611-628.

Montgomery, D.R., & Wohl, E.E. (2004). River and riverine landscapes. In: Gillespie, A.R., Porter, S.C., Atwater, B.F. (eds), *The Quaternary Period in the United States*, Developments in Quaternary Science 1, Elsevier Amsterdam, pp. 221-246.

Morgan, R. P. C. (1999). *Soil Erosion and Conservation*. In: Soil Erosion and Conservation. Blackwell Publishing, 45–65.

Nimmo, J. R., & Perkiins, K. S. (2002). *Aggregate Stability and Size Distribution.* in: Dane, J.H., Topp, G. C. (Eds.), Methods of Soil Analysis, Part 4 - Physical Methods. Soil Science Society of America, Madison, Wisconsin, 317–328.

Nishiizumi, K., Imamura, M., Caffee, M.W., Southon, J.R., Finkel, R.C., & McAnich, J. (2007). *Absolute calibration of ^{10}Be AMS standards.* Nuclear Instruments & Methods in Physics Research Section B-Beam Interactions with Materials and Atoms 258: 403-413. DOI: 10.1016/j.nimb.2007.01.297

Norton, K.P., von Blanckenburg, F., Kubik, P.W. (2010). Competition between diffusive and stochastic erosional processes and their rates derived from cosmogenic ^{10}Be in the glacially sculpted upper Rhone valley, Swiss Alps. *Earth Surface Processes and Landforms*, *35*, 651-662.

Parfitt, R. L., & Henmi, T. (1982). Comparison of an oxalate-extraction method and an infrared spectroscopic method for determining allophane in soil clays. *Soil Science and Plant Nutrition*, *28*, 183–190. doi:10.1080/00380768.1982.10432435

Pawlik, Ł. (2013). The role of trees in the geomorphic system of forested hillslopes — a review. *Earth-Science Reviews*, *126*, 250–265. doi:10.1016/j.earscirev.2013.08.007

Pawlik, Ł., Phillips, J. D., & Šamonil, P. (2016). Roots, rock, and regolith: biomechanical and biochemical weathering by trees and its impact on hillslopes – a critical literature review. *Earth-Science Reviews*, *159*, 142–159. doi:10.1016/j.earscirev.2016.06.002

Pawlik, Ł., & Šamonil, P. (2018). Soil creep: The driving factors, evidence and significance for biogeomorphic and pedogenic domains and systems – A critical literature review. *Earth Science Reviews*, 178, 257–278. doi:10.1016/j.earscirev.2018.01.008

Pavlíček, V. (2004). *Geology of the Novohradské hory Mts. (Geologie Novohradských hor)*. In: Kubeš, J., (ed.): Krajina Novohradských hor – fyzicko-geografické složky krajiny. Jihočeská univerzita Pedagogická fakulta, České Budějovice, 9–45.

Petrillo, M., Cherubini, P., Fravolini, G., Ascher, J., Schärer, M., Synal, H.-A., Barbero, A., Bertoldi, D., Camin, F., Larcher, R., & Egli, M. (2016). Time since death and decay rate constants of Norway spruce and European larch deadwood in subalpine forests determined using dendrochronology and radiocarbon dating. *Biogeosciences*, *13*, 1537–1552. doi:10.5194/bg-13-1537-2016

Phillips, J. D. (2009). Biological energy in landscape evolution. *American Journal of Science*, *309*, 271–290. doi:10.2475/04.2009.01

Pieri, C. J. M. (1992). *Fertility of soils: a future for farming in the West African savannah*. Springer-

Verlag, Berlin.

Průša, E. (1985). *Die böhmischen und mährischen Urwälder — ihre Struktur und Ökologie*, Vegetace ČSSR A15. Academia, Praha.

Raab, G., Scarciglia, F., Norton, K., Dahms, D., de Castro Portes, R., Christl, M., Ketterer, M., Ruppli, A., & Egli, M. (2018). Denudation variability of the Sila massif upland (Italy) from decades to millennia using ^{10}Be and $^{239+240}$Pu. *Land Degradation & Development*, *29*, 3736–3752. doi:10.1002/ldr.3120.

Riebe, C.S., Kirchner, J.W., & Finkel, R.C. (2004). Erosional and climatic effects on long-term chemical weathering in granitic landscapes spanning diverse climate regimes. *Earth and Planetary Science Letters, 224*, 546-562. doi:10.1016/j.epsl.2004.05.019

Román-Sánchez, A., Reimann, T., Wallinga, J., & Vanwalleghem, T. (2019). Bioturbation and erosion rates along the soil-hillslope conveyor belt, part 1: Insights from single-grain feldspar luminescence. *Earth Surface Processes and Landforms*, DOI: 10.1002/esp.4628.

Šamonil, P., Daněk, P., Senecká, A., Adam, D., & Phillips, J. D. (2018). The biomechanical effects of trees in a temperate forest. *Earth Surface Processes and Landforms*, *43*, 1063–1072. doi:10.1002/esp.4304

Šamonil, P., Daněk, P., Dušan, A., & Phillips, J. D. (2017). Breakage or uprooting: How tree death type affects hillslope processes in old-growth temperate forests. *Geomorphology*, *299*, 76–84. doi:10.1016/j.geomorph.2017.09.023

Šamonil, P., Daněk, P., Schaetzl, R. J., Vašíčková, I., & Valtera, M. (2015). Soil mixing and genesis as affected by tree uprooting in three temperate forests. *European Journal of Soil Science*, *66*, 589–603. doi:10.1111/ejss.12245

Šamonil, P., Vašíčková, I., Daněk, P., Janík, D., & Adam, D. (2014). Disturbances can control finescale pedodiversity in old-growth forests: Is the soil evolution theory disturbed as well? *Biogeosciences*, *11*, 5889–5905. doi:10.5194/bg-11-5889-2014

Šamonil, P., Schaetzl, R. J., Valtera, M., Goliáš, V., Bladrian, P., Vašíčková, I., Adam, D., Janík, D., & Hort, L. (2013). Crossdating of disturbances by tree uprooting: Can tree throw microtopography persist for 6000 years? *Forest Ecology and Management*, *307*, 123–135. doi:10.1002/esp.4304

Šamonil, P., Valtera, M., Bek, S., Šebkova, B., Vrška, T., & Houška, J. (2011). Soil variability through spatial scales in a permanently disturbed natural spruce-fir-beech forest. *European Journal of Forest Research*, *130*, 1075–191. doi:10.1007/s10342-011-0496-2

Sauer, D., Sponagel, H., Sommer, M., Giani, L., Jahn, R., & Stahr, K. (2007). Podzol: soil of the year 2007. A review on its genesis, occurrence, and functions. *Journal of Plant Nutrition and Soil Science*, *170*, 581–597. doi:10.1002/jpln.200700135

Schaetzl, R. J., & Follmer, L. R. (1990). Longevity of treethrow microtopography: implications for mass wasting. *Geomorphology*, *3*, 113–123. doi:10.1016/0169-555X(90)90040-W

Schaetzl, R. J., & Thompson, M. I. (2015). *Soils – Genesis and Geomorphology* (2nd Ed.). Cambridge University Press, 795 pp.

Šebková, B., Šamonil, P., Valtera, M., Adam, D., & Janík, D. (2012). Interaction between tree species populations and windthrow dynamics in natural beech-dominated forest, Czech Republic. *Forest Ecology and Management*, *280*, 9–19. doi:10.1016/j.foreco.2012.05.030

Šťava, O., Beneš, B., Brisbin, M., & Křivánek, J. (2008). Interactive terrain modeling using hydraulic erosion. In: *Proceedings of the 2008 ACM SIGGRAPH/Eurographics Symposium on Computer Animation*, 201–210.

Stone, J. (2000). Air pressure and cosmogenic isotope production. *Journal of Geophysical Research*, *105*, 23753–23760. doi:10.1029/2000JB900181

Strzyzowski, D., Fidelus-Orzechowska, J., & Zelazny, M. (2018). Sediment transport by uprooting in the forested part of the Tatra Mountains, southern Poland. *Catena*, 160, 329-338. 10.1016/j.catena.2017.09.019

Tolasz, R., Míková, T., Valeriánová, A., & Voženílek, V. (eds.), (2007). *Climate Atlas of Czechia*. Český hydrometeorologický ústav and Univerzita Palackého v Olomouci, Prague, Olomouc.

Walker, M. (2005). *Quaternary dating methods*. Wiley, Chichester. doi:10.1002/jqs.1053

Walling, D. E., & Quine, T. A. (1990). Calibration of caesium-137 measurements to provide quantitative erosion rate data. *Land Degradation and Rehabilitation*, *2*, 161–175. doi:10.1002/ldr.3400020302

Walling, D., & He, Q. (1999). *Improved models for estimating soil erosion rates from cesium-137 measurements*. *Journal of Environmental Quality, 28*, 611–622. DOI: 10.2134/jeq1999.00472425002800020027x

Waroszewski, J., Egli, M., Brandová, D., Christl, M., Kabala, C., Malkiewicz, M., Kierczak, J., Glina, B., & Jezierski, P., 2018. Identifying slope processes over time and their imprint in soils of medium-high mountains of Central Europe (the Karkonosze Mountains, Poland). *Earth Surface Processes and Landforms*, *43*, 1195-2012. DOI: 10.1002/esp.4305.

Wyshnytzky, C., Ouimet, W. B., McCarthy, J., Dethier, D. P., Shroba, R. R., Bierman, P. R., & Rood, D. H. (2015). Meteoric ^{10}Be, clay, and extractable iron depth profiles in the Colorado Front Range: Implications for understanding soil mixing and erosion. *Catena*, *127*, 32–45. doi:10.1016/j.catena.2014.12.008

Yu, F., Faybishenko, B., Hunt, A., & Ghanbarian, B. (2017). A simple model of the variability of soil depths. *Water*, *9*, 460; doi:10.3390/w9070460.

Zollinger, B., Alewell, C., Kneisel, C., Brandová, D., Petrillo, M., Plötze, M., Christl, M., & Egli, M. (2017). Soil formation and weathering in a permafrost environment of the Swiss Alps: a multi-parameter and non-steady-state approach. *Earth Surface Processes and Landforms*, *42*, 814–835. doi:10.1002/esp.4040

Table 1. Details about sampling sites and plots for short-term erosion measurements ($^{239+240}$Pu).

Site	Latitude (°N)	Longitude (°W)	Elevation (m a.s.l.)	Soil (IUSS Working Group WRB, 2014)	Type of plot	Replicates	Slope (°)
Soil-61	48.669	14.709	763	Dystric Cambisol	Slope	4	6
					Tree uprooting	4	18
					Reference	4	0
Soil-173	48.665	14.707	793	Albic Podzol	Slope	4	3
					Reference	4	0
Soil-177	48.664	14.708	801	Entic Podzol	Slope	4	10
					Reference	4	0

Table 2. Chemical and physical properties of the investigated soil profiles.

Plot No.	Soil horizon	Mean depth (cm)	Munsell colour (moist)	Oxalate extractable forms			Dithionite extractable forms		pH	Org. C	N	Density
				Al	Fe	Si	Al	Fe	H_2O			
				mg kg^{-1}			mg kg^{-1}			%	%	g cm^{-3}
61	A	0-5	10YR 3/2	3630	8273	312	3143	16936	4.03	ND	ND	ND
	ABw	5-15	10YR 4/3	5108	10226	237	4319	18476	4.46	5.95	0.40	0.71
	Bw1	15-30	10YR 5/4	6070	4141	766	4638	12297	4.84	2.34	0.17	0.79
	Bw2	30-50	10YR 5/3	5418	1690	962	3895	9100	4.94	1.34	0.09	0.85
	BC1	50-80	10YR 5/2	3968	803	751	2663	10511	4.91	0.94	0.07	0.98
	C1	80-100	10YR 5/3	2780	826	489	1852	8213	5.40	0.77	0.04	1.08
	C2	100-140	10YR 5/3	2750	952	550	2070	7670	5.20	0.36	0.02	1.04
	C3	140-160	10YR 5/3	1130	669	198	811	4400	5.10	ND	ND	ND
	C4	160-200	10YR 5/2	1510	446	326	1150	4400	5.20	ND	ND	ND
173	A	0-5	10YR 2/1	1552	1584	16	1439	2528	3.49	5.80	0.25	0.81
	E	5-10	7.5YR 6/1	832	162	10	517	1551	3.77	5.80	0.25	0.81
	Bhs	10-14	7.5YR 3/3	6749	19097	141	6459	25921	3.91	5.35	0.23	0.58
	Bs1	14-30	10YR 5/6	17993	14591	2518	13186	21825	4.55	5.44	0.18	0.67
	Bs2	30-50	10YR 6/4	16453	3200	4809	8343	9687	4.70	3.25	0.10	0.80
	BC1	50-100	7.5YR 5/1	1345	909	92	1100	6100	4.82	0.35	0.02	1.46
	C2	100-150	10YR 5/3	849	12510	96	621	5585	5.59	0.11	0.00	1.36
177	A	0-5	10YR 2/2	3701	20625	256	3538	20515	3.80	ND	ND	ND
	ABw	5-15	7.5YR 4/3	7440	10202	304	6176	27251	4.25	15.66	0.91	0.63
	Bs1	15-30	7.5YR 4/4	11660	8776	1226	10249	17061	4.61	4.29	0.22	0.71
	Bs2	30-50	7.5YR 6/6	10088	890	1581	7040	13889	4.54	1.75	0.09	ND
	BC1	50-100	10YR 5/3	4959	491	1117	2593	4011	4.87	0.52	0.03	0.85
	C1	100-150	10YR 5/3	2608	2237	549	1687	4296	4.91	0.09	0.00	1.30
	C2	150-160	10YR 5/3	ND	ND	ND	ND	ND	ND	ND	ND	ND

ND = not determined

Table 3. ^{10}Be measurements of the tor, rock, and soil samples of the Zofinsky Primeval Forest.

Sample name	Designation	Latitude (°N)	Longitude (°W)	Elevation (m a.s.l.)	Thickness (cm)	Shielding correction	Erosion rate[a] (cm yr^{-1})	[^{10}Be][b] (10^5 atoms g^{-1})	Measurement error (10^5 atoms g^{-1})	^{10}Be surface exposure age[d,e] (a)	Internal error (a)	External error (a)
ZOF-1	Tor_177 10cm	48.664	14.708	806	2.5	0.90	0.0001	7.17	0.247	100402	3862	9252
ZOF-2	Tor_177 100cm	48.664	14.708	806	2	0.976	0.0001	6.39	0.234	82786	3319	7565
ZOF-3	Tor_177 150cm	48.664	14.708	806	1.7	0.889	0.0001	6.81	0.230	97814	3678	8957
ZOF-4	Tor_177 210cm	48.664	14.708	806	1.8	0.983	0.0001	9.31	0.299	124015	4566	11600
ZOF-5	Tor_177 230cm	48.664	14.708	806	1.7	1	0.0001	9.30	0.308	121410	4596	11378
ZOF-7	Tor_177_2 10cm	48.664	14.709	806	1.5	0.499	0.0001	7.74	0.254	219491	9211	22978
ZOF-8	Tor_177_2 130cm	48.664	14.709	806	1.7	0.889	0.0001	1.02	0.331	154519	5951	14985
ZOF-9	Tor_177_2 215cm	48.664	14.709	806	1.7	0.998	0.0001	9.62	0.317	126369	4787	11900
ZOF-24	Tor_177_2 50cm (back side)	48.664	14.709	806	2.5	0.998	0.0001	9.62	0.317	115651	6298	11692
ZOF-10	Rock_177 -65cm	48.663	14.707	829	77[c]	0.998	0.0001	1.11	0.077	16032	1130	1658
ME142	Profile 61, Tor 10 cm	48.668	14.708	730	2	0.869	0.0001	1.08	0.042	15845	622	1360
ZOF-12	Profile 61, Tor 75 cm	48.668	14.708	730	2	0.631	0.0001	1.81	0.078	34228	1527	3071
ME143	Profile 61, Tor 110 cm	48.668	14.708	730	2	0.622	0.0001	2.36	0.068	49106	1490	4161
ZOF-13	Profile 61, Tor 135 cm	48.668	14.708	730	2	0.500	0.0001	2.75	0.102	67423	2692	6072
ME144	Profile 61, Tor 180 cm	48.668	14.708	730	2	0.714	0.0001	3.52	0.157	65080	3116	6097
Soil-61	Soil sample	48.669	14.709	763	10	1	-	2.48	0.230	-	-	-
Soil-173	Soil sample	48.665	14.707	793	10	1	-	2.09	0.110	-	-	-
Soil-177	Soil sample	48.664	14.708	801	10	1	-	1.96	0.131	-	-	-

[a] We used a density of 2.65 g cm^{-3} for all samples, an erosion rate of 1 mm kyr^{-1} and the 07KNSTD standard
[b] Uncertainty includes AMS measurements errors and statistical counting error
[c] soil material: a density of 1 g cm^{-3} was applied to correct for burial depth of 65 cm and rock sample thickness (see supplementary Table S1)
[d] Surface exposure ages were calculated with the CRONUS-Earth online calculators (http://hess.ess.washington.edu/, Balco et al., 2008 and version 3.0) and using scaling scheme for spallation based on Lal (1991)/Stone (2000)
[e] time-varying production rate model, Lal (1991)/Stone (2000)

Table 4. Results of Pu inventories and the erosion rates calculated with three different models. In addition, erosion rates determined from in-situ ^{10}Be (in soils) are given. Erosion rates using Pu were calculated with several models: PDM = profile distribution model, IM = inventory method and MODERN = modelling deposition and erosion rates with radionuclides (Arata et al., 2016). S = slope site and TUR = tree uprooting site.

Plot	Site	$^{239+240}$Pu					In-situ ^{10}Be
		PDM[a]	IM[b] P=1	IM[b] P=1.2	IM[b] P=1.5	MODERN[c]	
		(t km^{-2} yr^{-1})	(t km^{-2} yr^{-1})	(t km^{-2} yr^{-1})	(t km^{-2} yr^{-1})	(t km^{-2} yr^{-1})	(t km^{-2} yr^{-1})
61	S	-111	-111	-102	-81	-149	-58.0±7.2
	TUR	-136	-166	-147	-118	-196	
173	S	-83	-64	-59	-47	-68	-71.3±6.8
177	S	109	125	98	79	105	-76.3±8.0

Negative values = Erosion, Positive values = Deposition
[a]Walling & He (1999)
[b]Lal et al. (2013)
[c]Arata et al. (2016)

841 **Table 5.** MWD (mean weighted diameter) results of aggregates and derived categories of stability
842 (determined according to Le Bissonnais (1996) and Chenu et al. (2011)).
843

Profile	MWD (Le Bissonnais, 1996)	MWD (Chenu et al., 2011)
61	2.04	2.37
173	1.99	2.32
177	2.06	5.68
Significance		
very unstable	< 0.4	
unstable	0.4 - 0.8	
medium	0.8 - 1.3	
stable	1.3 - 2.0	
very stable	> 2.0	

844
845

Table 6. Meteoric ^{10}Be and physical parameters necessary to calculate the stocks.

Profile	Horizon	Depth (cm)	Thickness (cm)	Density (g cm^{-3})	Weight (g cm^{-2})	[^{10}Be] (10^8 atoms g^{-1})	Measurement error (%)	Measurement error (10^8 atoms g^{-1})	Skeleton content (wt-%)
61	Ah(Bv)	0-15	15	0.71	10.575	2.77	2.00%	0.05	26
	Bv	15-30	15	0.79	11.910	5.16	2.00%	0.10	28
	Bv	30-50	20	0.85	16.920	5.78	2.00%	0.12	33
	BvC1	50-80	30	0.98	29.340	3.74	2.00%	0.07	29
	C1	80-100	20	1.08	21.660	6.25	2.00%	0.13	30
	C2	100-140	40	1.04	41.400	4.04	2.00%	0.08	30
173	Ah/E	0-10	10	0.81	8.100	0.28	2.36%	0.01	9
	Bhs	10-14	4	0.58	2.320	0.63	2.02%	0.01	26
	Bs	14-30	16	0.67	10.640	3.75	2.00%	0.08	24
	Bs	30-50	20	0.80	15.920	3.87	2.00%	0.08	33
	BsC1	50-100	50	1.46	73.100	2.81	2.00%	0.06	36
	C2	100-150	50	1.36	68.150	0.83	2.02%	0.02	45
177	AhBvs	0-15	15	0.63	9.435	1.26	2.01%	0.03	19
	Bvs	15-30	15	0.71	10.635	6.53	2.00%	0.13	39
	Bvs/BvsC	30-100	70	0.85	59.430	4.57	2.00%	0.09	39
	C	100-160	60	1.30	77.700	0.29	2.26%	0.01	42

Table 7. Tree uprooting frequency, related uprooted soil material and potential amount susceptible to be eroded and deposited along the slope.

Period	Frequency (event ha^{-1} yr^{-1})	Mound volume (m^3 ha^{-1} yr^{-1})	Potential denudation volume (m^3 ha^{-1} yr^{-1})
1975–1997	0.63	1.22	0.48
1997–2008 (containing the Kyrill storm)	3.30	10.27	4.54
2008–2018	0.60	1.15	0.48
1975–2018 (corrected by weighing the Kyrill storm as a century event)	1.30	3.52	1.52

Figure captions

Figure 1. Overview of the investigation area (Zofin primeval forest), geological units and the sampling sites (soil sites and tors).

Figure 2. Sampled soil profiles, an example of a tree uprooting and investigated tors.

Figure 3. Surface ages as a function of height above the present-day surface of the three sampled tors.

Figure 4. a–c) exposure age – height trend simulation (linear, polynomial and logistic function) for tor 61 using a Monte Carlo approach, d–e) exposure age – height trend simulation (linear, and logistic function; polynomial function was not possible) for tor 177 using a Monte Carlo approach. Derived denudation rates over time for f) tor 177 (red lines: rates derived from the logistic function; grey area: rates derived from the linear function) and e) for tor 61 (red lines: rates derived from the logistic function; blue lines: rates derived from the polynomial function; grey area: rates derived from the linear function). Statistically different (ANOVA) R^2 values are indicated by * ($p < 0.05$) and ** ($p < 0.01$)

Figure 5. $^{239+240}$Pu inventories of the investigated sites (each having 4 replicates). a) Profile 61 with erosional, tree uprooting (TUR) and reference site, b) Profile 173 with slope and reference site, c) Profile 177 with accumulation and reference site.

Figure 6. Meteoric ^{10}Be distribution along the soil profiles a) Profile 61, b) Profile 173, c) Profile 177.

Figure 7. Modelling of soil ages (meteoric ^{10}Be) as a function of precipitation rates. The rectangles indicate the most probable age range of the individual soils.

Figure 8. a) Example of a tree uprooting event that was monitored with the tree throw census, b) proportion of soil material that falls back into the pit as a function of treefall and slope angle.

Figure 9. Correlation between the different model approaches to calculate soil mass redistribution (erosion or accumulation); a) correlation between MODERN and the inventory method (IM) or the profile distribution model (PDM), b) correlation between IM and PDM.

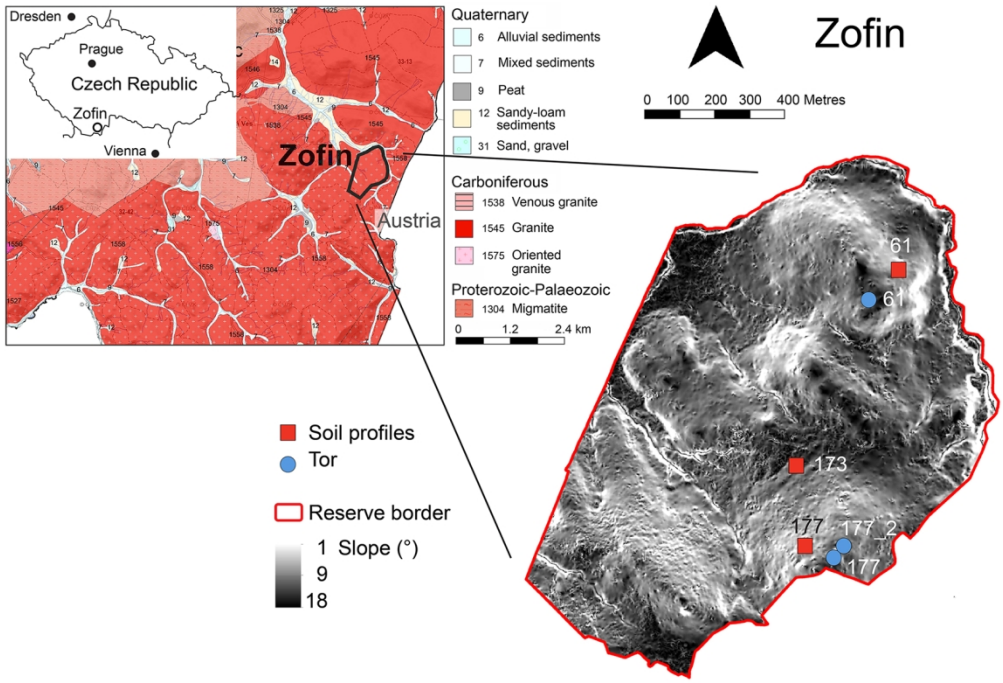
Dresden
Prague
Czech Republic
Zofin
Vienna
Zofin
Austria
Quaternary
6 Alluvial sediments
7 Mixed sediments
9 Peat
12 Sandy-loam sediments
31 Sand, gravel
Carboniferous
1538 Venous granite
1545 Granite
1575 Oriented granite
Proterozoic-Palaeozoic
1304 Migmatite
0 1.2 2.4 km
Zofin
0 100 200 300 400 Metres
Soil profiles
Tor
Reserve border
1 Slope (°)
9
18
61
61
173
177
177_2
177

Figure 1


O
A
ABw
Bw
BC1
C1
C2
C3
Profile 61
A
E
Bhs
Bs
BC1
C2
Profile 173
A
ABw
Bs
BC1
C1
C2
Profile 177
Tor 61
Tree uproot
Tor 177
Tor 177_2

Figure 2

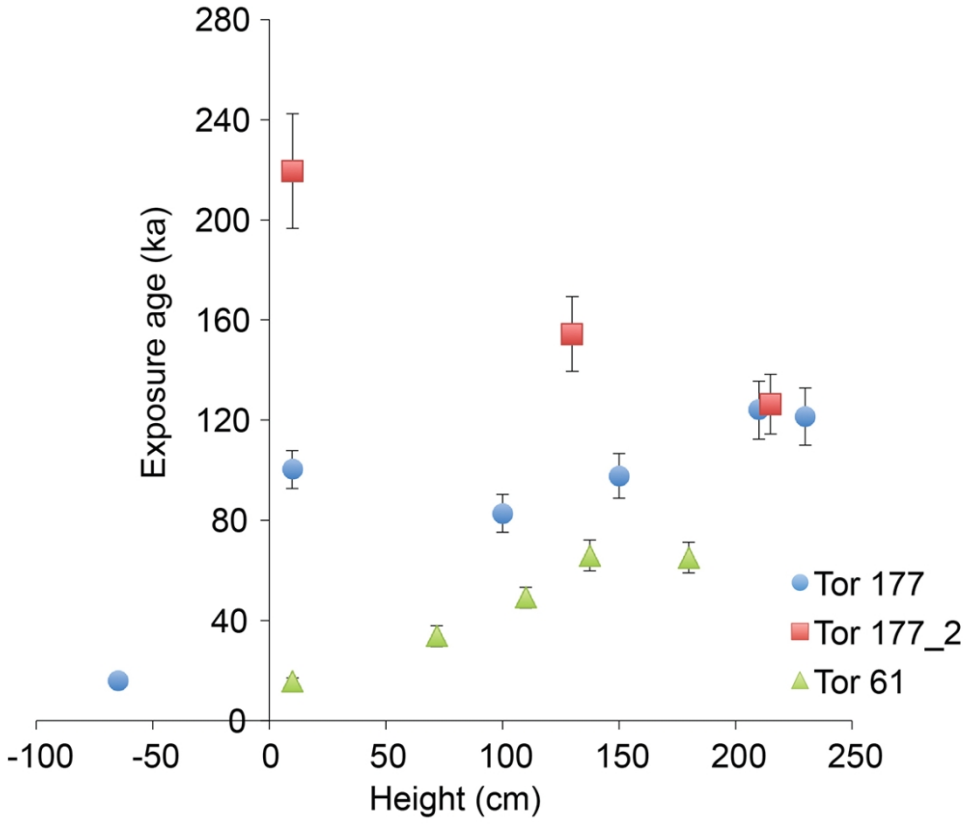
280
240
200
160
120
80
40
0
Exposure age (ka)
-100
-50
0
50
100
150
200
250
Height (cm)
Tor 177
Tor 177_2
Tor 61

Figure 3

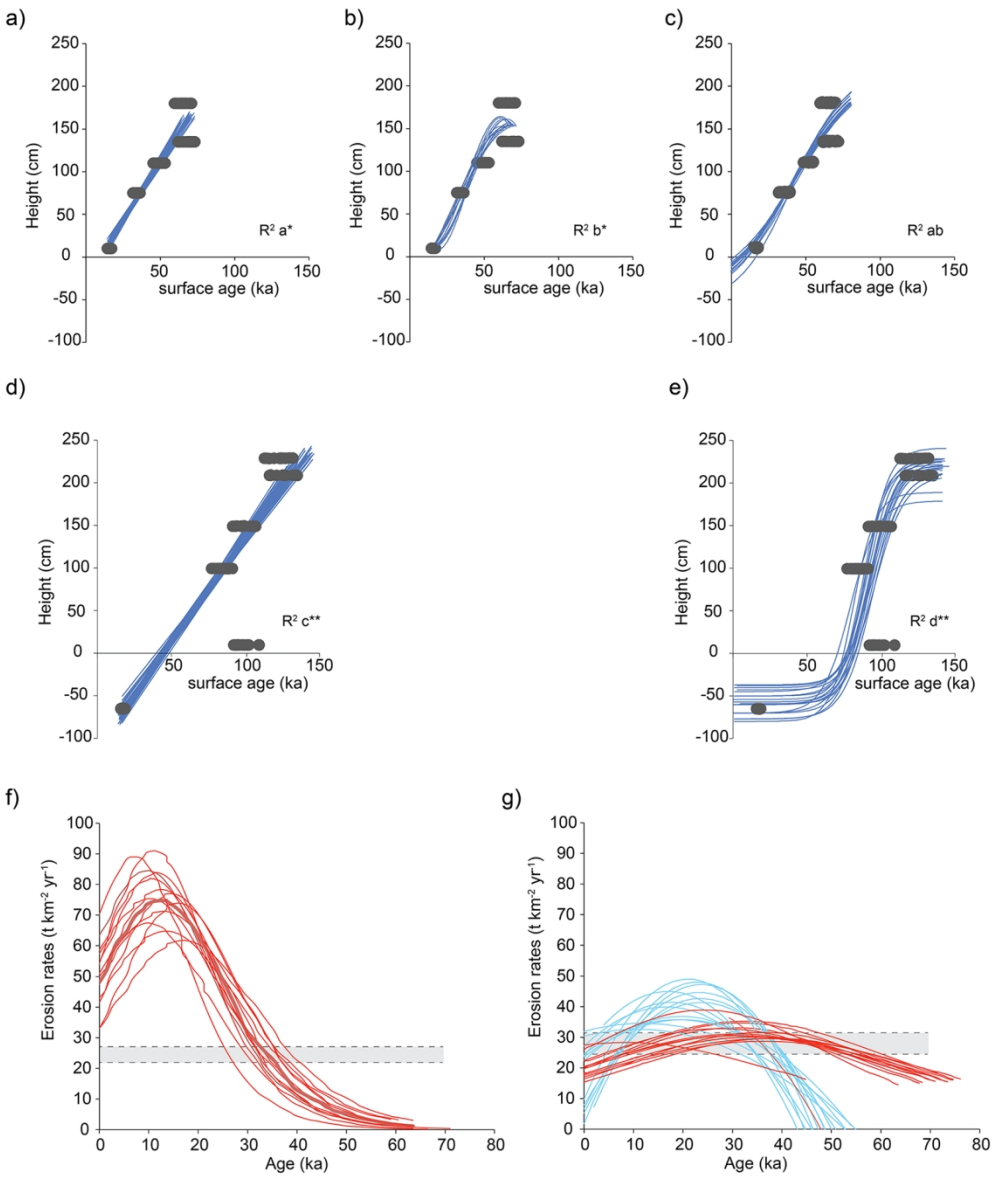
a)
b)
c)
d)
e)
f)
g)
Height (cm)
surface age (ka)
R² a*
R² b*
R² ab
R² c**
R² d**
Erosion rates (t km⁻² yr⁻¹)
Age (ka)

Figure 4

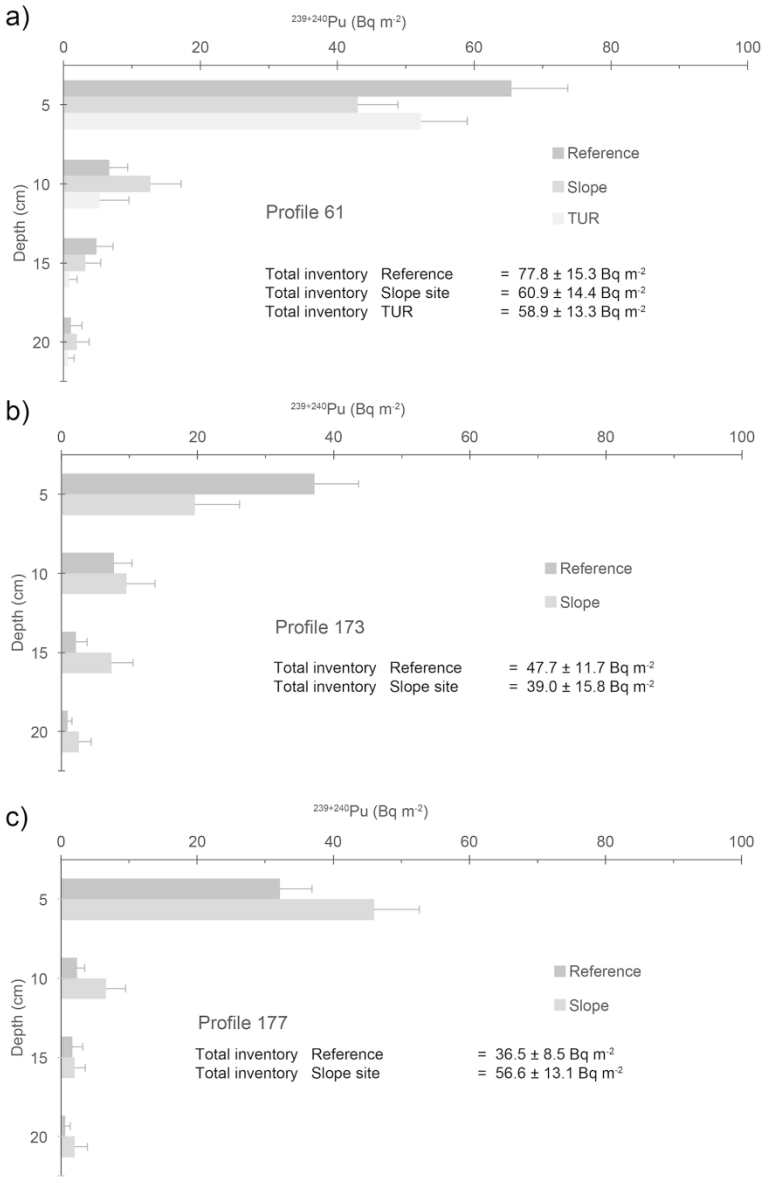
a)
$^{239+240}$Pu (Bq m^{-2})
0
20
40
60
80
100
5
10
15
20
Depth (cm)
Reference
Slope
TUR
Profile 61
Total inventory Reference = 77.8 ± 15.3 Bq m^{-2}
Total inventory Slope site = 60.9 ± 14.4 Bq m^{-2}
Total inventory TUR = 58.9 ± 13.3 Bq m^{-2}
b)
$^{239+240}$Pu (Bq m^{-2})
Reference
Slope
Profile 173
Total inventory Reference = 47.7 ± 11.7 Bq m^{-2}
Total inventory Slope site = 39.0 ± 15.8 Bq m^{-2}
c)
$^{239+240}$Pu (Bq m^{-2})
Reference
Slope
Profile 177
Total inventory Reference = 36.5 ± 8.5 Bq m^{-2}
Total inventory Slope site = 56.6 ± 13.1 Bq m^{-2}

Figure 5

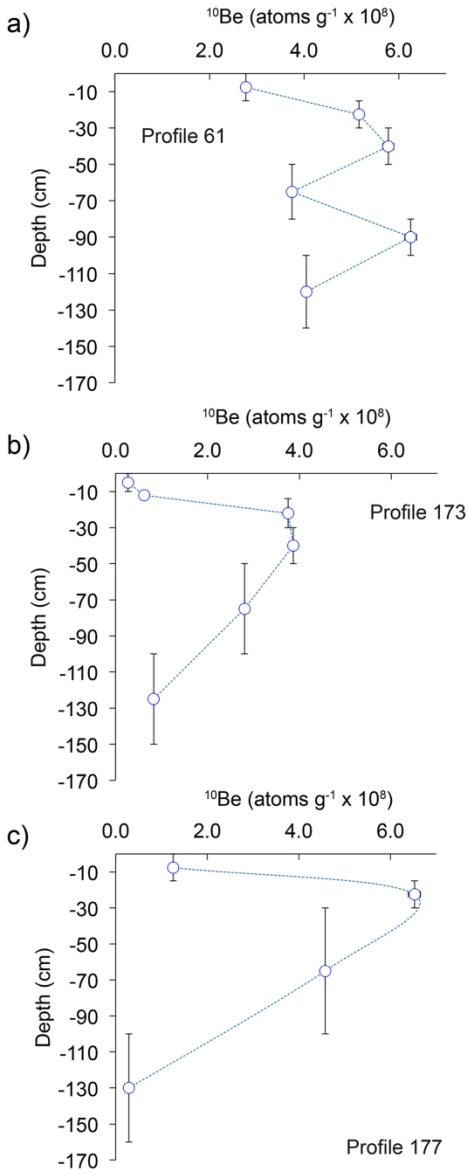
a)
^{10}Be (atoms g^{-1} x 10^{8})
0.0
2.0
4.0
6.0
-10
-30
-50
-70
-90
-110
-130
-150
-170
Depth (cm)
Profile 61
b)
^{10}Be (atoms g^{-1} x 10^{8})
0.0
2.0
4.0
6.0
-10
-30
-50
-70
-90
-110
-130
-150
-170
Depth (cm)
Profile 173
c)
^{10}Be (atoms g^{-1} x 10^{8})
0.0
2.0
4.0
6.0
-10
-30
-50
-70
-90
-110
-130
-150
-170
Depth (cm)
Profile 177

Figure 6

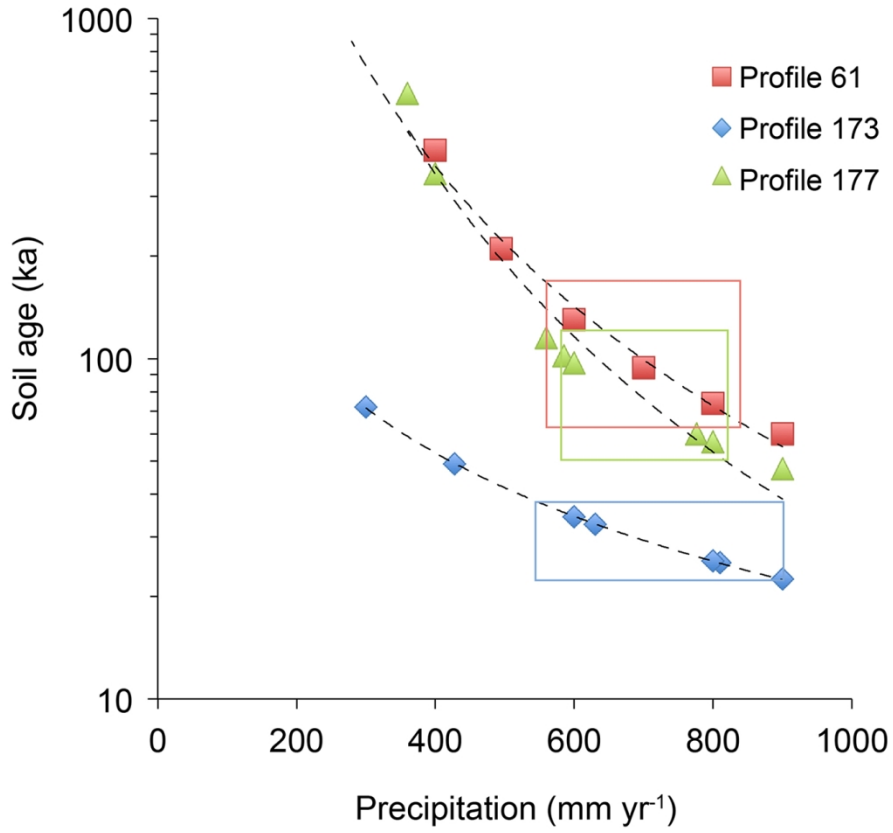
1000
100
10
Soil age (ka)
0
200
400
600
800
1000
Precipitation (mm yr-1)
Profile 61
Profile 173
Profile 177

Figure 7

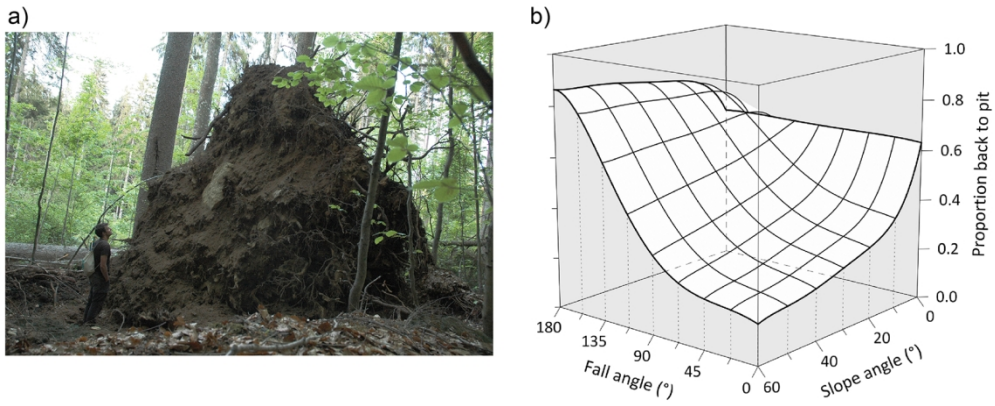
a)
b)
1.0
0.8
0.6
0.4
0.2
0.0
Proportion back to pit
180
135
90
45
0
Fall angle (°)
0
20
40
60
Slope angle (°)

Figure 8

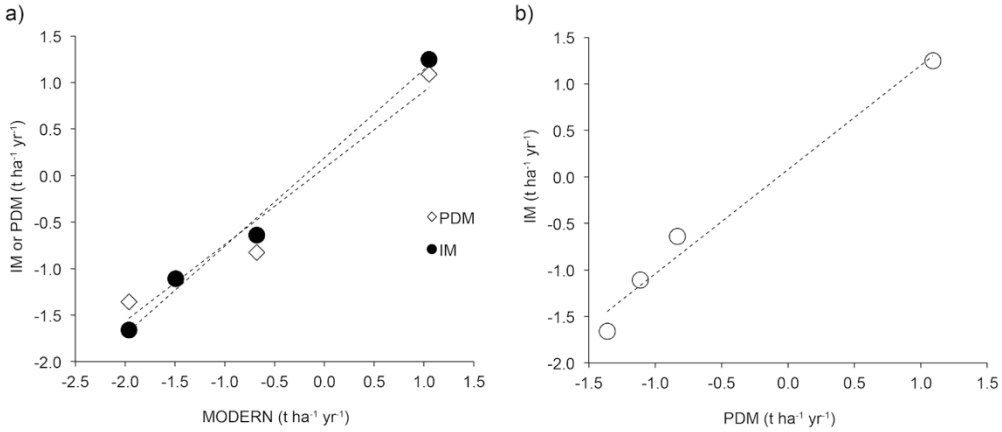
a)
b)
IM or PDM (t ha-1 yr-1)
MODERN (t ha-1 yr-1)
PDM
IM
IM (t ha-1 yr-1)
PDM (t ha-1 yr-1)

Figure 9